

# MMS-VPR: Multimodal Street-Level Visual Place Recognition Dataset and Benchmark

Yiwei Ou<sup>†</sup>, Xiaobin Ren<sup>†</sup>, Ronggui Sun<sup>†</sup>, Guansong Gao<sup>†</sup>, Kaiqi Zhao<sup>§</sup>, Manfredo Manfredini<sup>†</sup>  
<sup>†</sup>The University of Auckland    <sup>§</sup>Harbin Institute of Technology, Shenzhen

## Abstract

Existing visual place recognition (VPR) datasets predominantly rely on vehicle-mounted imagery, offer limited multimodal diversity, and underrepresent dense pedestrian street scenes, particularly in non-Western urban contexts. We introduce MMS-VPR, a large-scale multimodal dataset for street-level place recognition in pedestrian-only environments. MMS-VPR comprises 110,529 images and 2,527 video clips across 208 locations in a ~70,800 m<sup>2</sup> open-air commercial district in Chengdu, China. Field data were collected in 2024, while social media data span seven years (2019-2025), providing both fine-grained temporal granularity and long-term temporal coverage. Each location features comprehensive day-night coverage, multiple viewing angles, and multimodal annotations including GPS coordinates, timestamps, and semantic textual metadata. We further release MMS-VPRLib, a unified benchmarking platform that consolidates commonly used VPR datasets and state-of-the-art methods under a standardized, reproducible pipeline. MMS-VPRLib provides modular components for data pre-processing, multimodal modeling (CNN/RNN/Transformer), signal enhancement, alignment, fusion, and performance evaluation. This platform moves beyond traditional image-only paradigms, enabling systematic exploitation of complementary visual, video, and textual modalities<sup>1</sup>.

## ACM Reference Format:

Yiwei Ou<sup>†</sup>, Xiaobin Ren<sup>†</sup>, Ronggui Sun<sup>†</sup>, Guansong Gao<sup>†</sup>, Kaiqi Zhao<sup>§</sup>, Manfredo Manfredini<sup>†</sup>, <sup>†</sup>The University of Auckland    <sup>§</sup>Harbin Institute of Technology, Shenzhen . 2026. MMS-VPR: Multimodal Street-Level Visual Place Recognition Dataset and Benchmark. In . ACM, New York, NY, USA, 16 pages. <https://doi.org/10.1145/nnnnnnn.nnnnnnn>

## 1 Introduction

Visual Place Recognition (VPR), also known as visual geolocalization, is employed to retrieve visually similar locations from geotagged image databases, thereby estimating the approximate geographic position of a given query image [48, 82]. In recent years, VPR datasets have received increasing attention across diverse fields, including geography, computer vision, robotics, autonomous driving, and urban studies [40, 64, 82, 84].

<sup>1</sup>The dataset is available at <https://huggingface.co/datasets/Yiwei-Ou/MMS-VPR>. The benchmark is available at <https://github.com/yiasun/MMS-VPRLib> Preprint. Under review.

Permission to make digital or hard copies of all or part of this work for personal or classroom use is granted without fee provided that copies are not made or distributed for profit or commercial advantage and that copies bear this notice and the full citation on the first page. Copyrights for components of this work owned by others than the author(s) must be honored. Abstracting with credit is permitted. To copy otherwise, or republish, to post on servers or to redistribute to lists, requires prior specific permission and/or a fee. Request permissions from [permissions@acm.org](mailto:permissions@acm.org).  
*Conference'17, Washington, DC, USA*

© 2026 Copyright held by the owner/author(s). Publication rights licensed to ACM.  
ACM ISBN 978-x-xxxx-xxxx-x/YYYY/MM  
<https://doi.org/10.1145/nnnnnnn.nnnnnnn>

Current VPR datasets face four critical limitations that hinder their applicability to real-world urban scenarios (Figure 1). **First, vehicle-mounted perspective:** Most existing datasets rely on vehicle-mounted cameras (Google Maps, Baidu Maps, Mapillary) [1, 41], excluding pedestrian-only spaces inaccessible to vehicles. Although some studies consider pedestrian contexts [13, 14, 58, 71], they focus on sparsely distributed areas or small institutional campuses, overlooking dense commercial districts with high pedestrian traffic and visual complexity [30, 60, 86]. **Second, daytime-based collection:** Temporal coverage is limited—most datasets capture only daytime conditions, lacking diverse lighting environments necessary for robust recognition under varying illumination [51, 62]. **Third, unimodality:** Most datasets rely exclusively on single-modality visual inputs, overlooking complementary information from other modalities. While vision foundation models (VFMs) such as CLIP [65] and DINO [16] have shown remarkable performance on clean, controlled datasets (e.g., ImageNet [23]), they lack multimodal knowledge necessary for handling complex urban environments with severe occlusions, dynamic lighting, and visual ambiguity [8]. Recent studies [44, 50] have begun exploring multimodal fusion, but additional modalities such as textual descriptions, street-level videos, and spatial structure information—particularly in visually cluttered pedestrian settings—remain largely unexplored. **Fourth, limited temporal span:** Existing datasets typically cover short time periods (weeks to months) and are sensitive to seasonal variations, lacking the extended multi-year temporal coverage necessary for modeling long-term environmental changes [70].

To address these limitations, we introduce MMS-VPR with four characteristics (Figure 1): **(1) Pedestrian-only streets**—systematic field collection in dense commercial districts inaccessible to vehicles, providing human-centric viewpoints for AR and navigation applications; **(2) Day & night coverage**—balanced temporal sampling across daytime (7AM-5PM) and nighttime (6PM-10PM) periods, enabling illumination-robust place recognition; **(3) Multimodality**—integration of images, videos, and rich textual annotations (GPS coordinates, spatial identifiers, shop names/signage, street properties, space syntax metrics), organized in an explicit graph structure supporting diverse learning paradigms; **(4) Long temporal span**—combining systematic field collection (2024) with seven years of social media data (2019-2025), providing both fine-grained temporal granularity and extended coverage for modeling urban evolution. As shown in Table 1, these features position MMS-VPR distinctively among existing VPR datasets and benchmarks.

Our main contributions are summarized as follows:

- We present **MMS-VPR**, the first multimodal street-level VPR dataset systematically integrating images, videos, and text with comprehensive day-night coverage and 7-year temporal span in dense pedestrian-only environments. The dataset contains 110,529 images and 2,527 videos across 208 locations, with rich

textual annotations including GPS coordinates, store names (e.g., *Starbucks*), OCR-extracted signage, and space syntax metrics (from city science) organized in an explicit graph structure.

- We develop **MMS-VPRLib**, an open-source benchmark platform providing standardized pipelines for multimodal VPR with modular support for diverse architectures, signal enhancement, alignment and fusion strategies. Unlike existing benchmarks, MMS-VPRLib incorporates state-of-the-art Transformer-based and multimodal methods. The platform unifies widely used datasets (Pittsburgh [77], Tokyo 24/7 [76], Nordland [75]) with our MMS-VPR dataset under a consistent interface, enabling fair comparison and easy extension to new datasets and methods.
- Extensive experiments on *MMS-VPRLib* with 17 baseline models across 6 datasets demonstrate the effectiveness of *MMS-VPRLib* as a comprehensive evaluation benchmark and provide systematic insights into model performance, efficiency trade-offs, and hyperparameter sensitivity for multimodal VPR tasks.

## 2 Data Collection Methods

As presented in Figure 1, our data collection methodology addresses the four identified limitations through a systematic framework integrating pedestrian-level capture, balanced day-night coverage, multimodal data sources, and extended temporal span. The complete pipeline (Figure 2) encompasses four stages: site collection, data processing, textual annotation, and social media integration.

### 2.1 Site Selection

We selected Chengdu Taikoo Li, a  $\sim 70,800$  m<sup>2</sup> open-air commercial district in Chengdu’s CBD, China (Figure 1), as our data collection site. This location exemplifies dense pedestrian-only urban environments with three key characteristics: (1) *spatial openness* supporting diverse environmental conditions (lighting, weather, crowd density) and varied pedestrian activities; (2) *functional diversity*—retail, dining, leisure, cultural spaces—ensuring rich spatial semantics and consistent pedestrian traffic; (3) *urban integration* with surrounding urban streets, forming a context similar to pedestrianized districts worldwide. Detailed site information is provided in Appendix B.2.

### 2.2 Data Collection Framework

To enable reproducibility and facilitate similar dataset creation in other cities, we propose a systematic framework for acquiring multimodal street-level data in dense pedestrian environments (Figure 2). Our methodology uses accessible smartphones (iPhone XS Max, 11 Pro Max) for visual capture, with 4032×3024 image and 1920×1080 video resolution (30fps) ensuring both quality and accessibility.

**Site Collection.** Following our systematic data collection principles (Section 2.3), we conducted comprehensive field surveys capturing 1,417 high-resolution images and 747 videos (21.4 hours total) using smartphone cameras. The raw data totaled over 90GB.

**Data Processing.** We applied resolution standardization, extracted video frames at 1Hz, and performed data cleaning to remove non-useful captures. This processing stage generated the final field-collected dataset of 78,575 images and 2,527 video clips.

**Textual Annotation.** Each location received comprehensive annotations including: place ID and graph encoding (e.g., "Eh-5-3"),

**Table 1: MMS\_VPR positioning in VPR landscape. Panel A compares datasets; Panel B compares benchmark platforms. ✓: supported; ●: limited; ✗: not provided**

Panel A: Dataset Comparison								
Dataset	Modality			Robustness			Level	
	Img	Vid	Txt	Day-night	Multi-angles	Time span	Granularity	Pedestrian
Tokyo 24/7 [76]	✓	✗	✗	✓	✗	2 years	min-hr	✓
Pittsburgh [77]	✓	✗	✗	✗	✓	0.5 years	sec-min	✓
New College [74]	✓	✗	✗	✗	✓	✗	sec	✗
Nordland [75]	✓	✗	✗	●	✗	1 year	1s	✓
Cambridge [43]	✓	✗	✗	✓	✓	1 year	min-hr	●
<b>MMS_VPR (ours)</b>	✓	✓	✓	✓	✓	7 years	1-10s	✓

Panel B: Benchmark Platform Comparison								
Benchmark	Modality			Model architecture				Platform
	Img	Vid	Txt	CNN	RNN	Transformer	Multimodal	Integration
VPR-Bench [89]	✓	✗	✗	✓	✓	✗	✗	✓
VPR-Ensem [26]	✓	✗	✗	✓	✓	✗	✗	✓
<b>MMS_VPRLib (ours)</b>	✓	✓	✓	✓	✓	✓	✓	✓

**Table 2: Comparison of data collection strategies.**

Dataset	Viewpoint	Perspective	Day/Night	Evidence Base
Google Street View [4]	360° panorama	Single (elevated)	Limited	Vehicle coverage
Mapillary [56]	Opportunistic	Variable	Opportunistic	Crowdsourcing
RobotCar [51]	Forward-facing	Single (vehicle)	Systematic	Autonomous driving
Pittsburgh [77]	Panoramic	Single	Daytime only	Street-view mining
Nordland [75]	Forward-facing	Single (rail)	Seasonal	Railway traverse
<b>MMS-VPR (ours)</b>	<b>4 directions</b>	<b>Dual (0°, 45°)</b>	<b>Balanced</b>	<b>Human vision [57] + VPR studies [49] + Social media [33]</b>

GPS, shop names and visible signage extracted via OCR and manual verification, physical street properties (width, length), and space syntax metrics quantifying spatial configuration (Section 3.3).

**Social Media Integration.** To extend temporal coverage, we collected 31,954 images from Weibo (Chinese Twitter) using keyword "Chengdu Taikoo Li" spanning 2019-2025 (30GB+ data). Social media imagery has been widely adopted to augment VPR datasets with diverse temporal and viewpoint variations [17, 33]. The integrated visual-place matching across field and social media data creates a total of 110,529 images and 2,527 videos, providing both fine-grained temporal granularity and 7-year extended coverage.

### 2.3 Data Collection Principles

Our methodology is grounded in three evidence-based principles addressing critical factors affecting VPR performance: viewpoint variation [49, 91], illumination changes [51, 62], and temporal dynamics [70]. Table 2 positions our approach against existing datasets, with detailed implementation protocols provided in Appendix B.3.

**Principle 1: Four-Direction Coverage.** Existing research [91] shows that VPR performance degrades by up to 40% when query viewpoints differ from training viewpoints. Thus, we systematically capture from four cardinal directions (N, S, E, W) for each street, ensuring balanced viewpoint coverage that matches real-world usage patterns. We choose discrete directional captures over 360° panoramas because: (1) panoramic imagery introduces geometric distortions [76]; (2) users rarely capture panoramas; (3) multi-perspective discrete captures provide superior VPR performance [70].

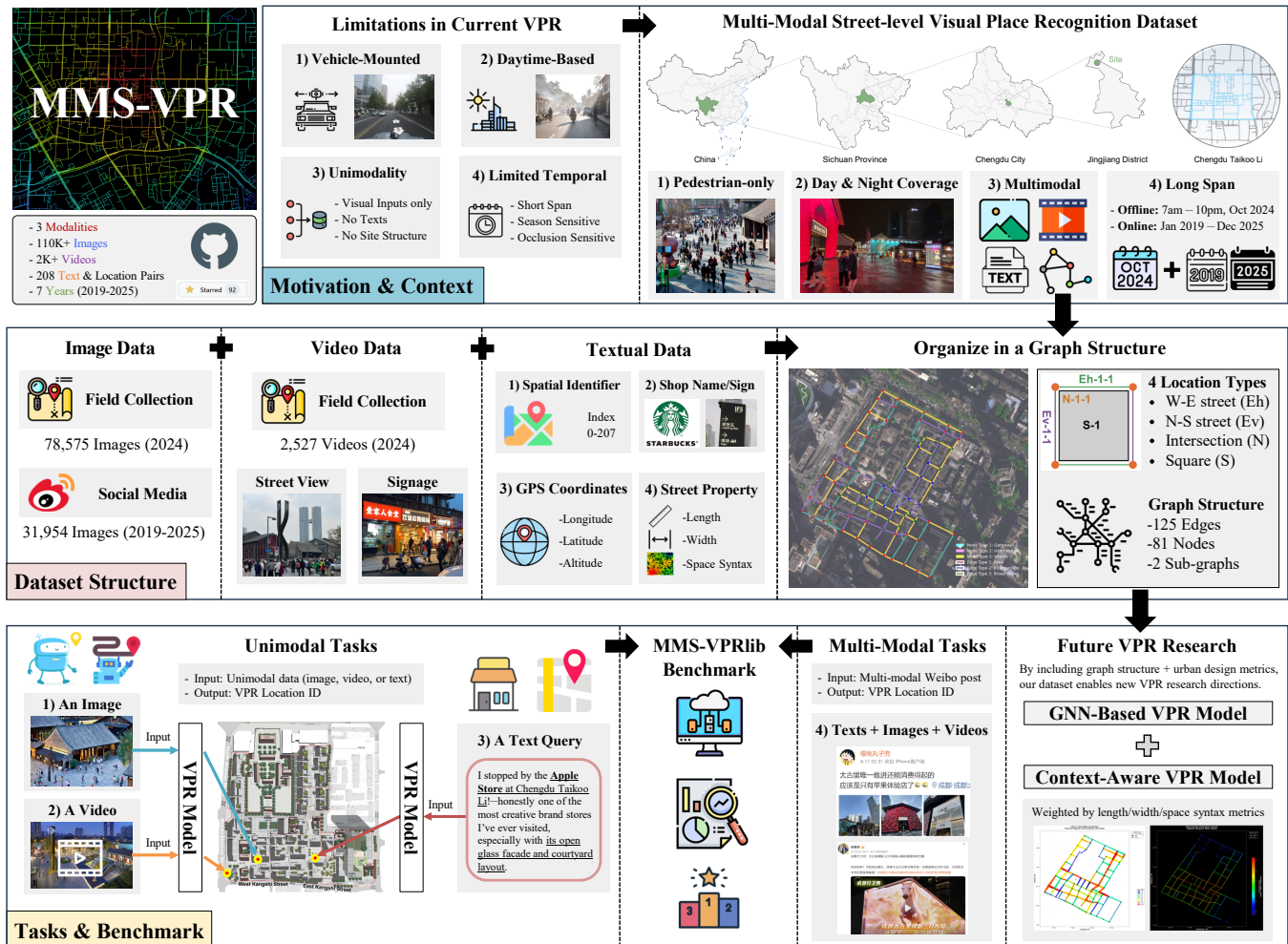


Figure 1: Overview of MMS-VPR framework addressing four VPR limitations through pedestrian-only urban environments data collection, day-night coverage, multimodal integration, and 7-year temporal span enhanced with social media data.

**Principle 2: Dual-Perspective Capture.** Research on human visual field structure shows that pedestrians naturally employ two viewing strategies in high-rise environments: forward-looking (0°) for navigation and upward-looking (30-60°) for landmark recognition [22, 57]. The human visual field spans approximately 120° horizontal and 60° vertical [69], while smartphone cameras provide narrower coverage (iPhone: 65° horizontal, 46° vertical [6]). In VPR contexts, incorporating upward-facing imagery improves place recognition recall by 15-30% in urban environments where building facades provide primary discriminative features [31]. We capture each view with two perspectives: horizontal (0°) and upward (45°), calibrated to capture both eye-level features and upper-level architectural details that serve as stable, occlusion-resistant landmarks.

**Principle 3: Balanced Day-Night Coverage.** Illumination variation represents one of the most significant VPR challenges, with studies reporting 50-80% performance drops when deploying daytime-trained models on nighttime queries [5, 62]. Analysis of social media photographs from commercial districts reveals that 55-65% are

captured during evening hours [63], reflecting actual usage patterns. We enforce balanced temporal coverage with equivalent data volume during daytime (7AM-5PM) and nighttime (6PM-10PM) periods. Our fine-grained temporal sampling captures lighting dynamics that enable models to learn robust representations across the full illumination spectrum rather than discrete snapshots [79].

### 2.4 Dual-Source Data Integration

**Field Collection (2024).** Systematic on-site data collection yielded 78,575 images and 2,527 video clips across 208 locations, providing comprehensive spatial coverage with fine temporal granularity across 7AM-10PM and variations in pedestrian occlusion patterns.

**Social Media Integration (2019-2025).** To address the limited temporal span of field collection, we curated 31,954 georeferenced images from Weibo (Chinese Twitter) posted at these 208 locations between January 1, 2019 and December 31, 2025. This seven-year span enables robust modeling of long-term environmental changes

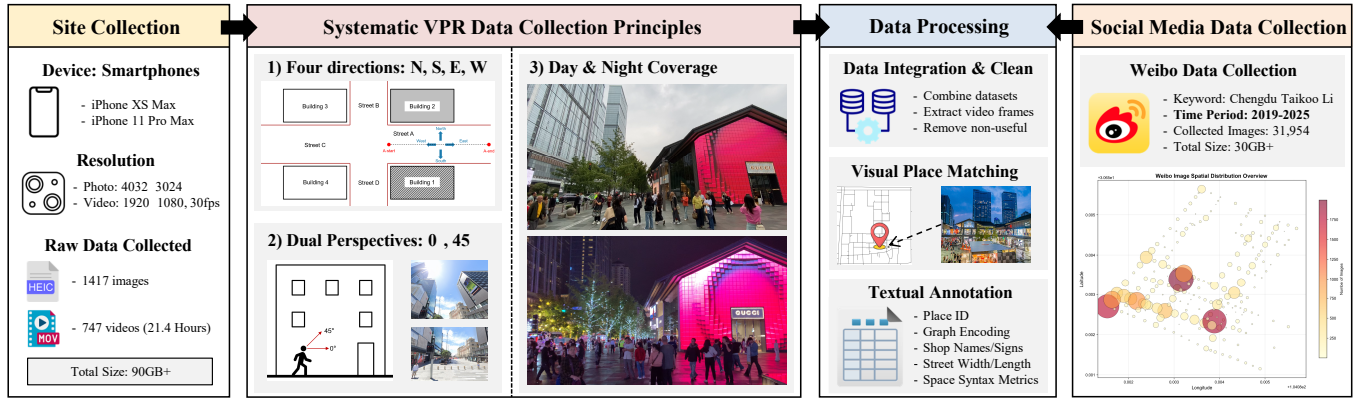


Figure 2: Pipeline for building MMS-VPR: site collection, data processing, textual annotation, and social media integration.

(seasonal variations, architectural modifications, evolving urban dynamics) while maintaining spatial consistency with field data.

**Combined Dataset Statistics.** The integrated dataset contains **110,529 images** and **2,527 videos** across **208 unique place classes**, providing both fine-grained temporal coverage and extended temporal span unprecedented in pedestrian-level VPR datasets.

### 3 MMS-VPR Dataset

#### 3.1 Multimodal Data Composition

MMS-VPR comprises three complementary data modalities unified through an explicit spatial graph structure, enabling multimodal place recognition and graph-based learning approaches.

**Image Data.** 110,529 georeferenced images from dual sources: (1) *Field-collected*—78,575 images including still photographs and 1Hz-extracted frames, providing comprehensive coverage under day-night and multi-perspective protocols; (2) *Social media*—31,954 curated photographs from Weibo (2019–2025), offering viewpoint diversity and seven-year temporal extent. Resolution ranges from 4032×3024 (original) to 256×192 (preprocessed).

**Video Data.** Field collection yielded 2,527 video clips (20–60 seconds, 1920×1080 at 30fps) recorded along streets from multiple directions during day-night periods. Videos provide motion dynamics absent in still images, supporting video-based motion-aware place recognition using recurrent architectures (LSTM, GRU) or temporal convolutions (3D-CNN, Video Transformers).

**Textual Data.** Each location is annotated with: (1) *Spatial identifiers*—systematic encodings preserving graph topology, enabling adjacency matrix construction for GNN applications; (2) *Visible signage*—discriminative store names and landmark text extracted via OCR and manually verified, providing semantic anchors for text-based retrieval. Example inventory: "Starbucks, Adidas, LEGO"; (3) *GPS coordinates*—the longitude and latitude of each VPR location; (4) *Spatial configuration metrics*—described in Section 3.3.

**Graph Structure Integration.** All 208 locations are organized in a spatial graph  $G = (V, E)$  representing the pedestrian network topology. We provide complete graph connectivity tables specifying edge connections, shared nodes, turning angles, and distance metrics, enabling direct graph construction for GNN-based methods.

Table 3: Dataset statistics by spatial type. Combined field collection and social media data across 208 locations.

Spatial Type	Index	Classes	Images	Videos	Avg./Location
Nodes	0–80	81	47,049	1,197	580.85
Squares	81–82	2	5,686	7	2,843.00
Horizontal Edges	83–143	61	28,178	662	461.93
Vertical Edges	144–207	64	29,616	646	462.75
<b>Total</b>	<b>0–207</b>	<b>208</b>	<b>110,529</b>	<b>2,527</b>	<b>531.39</b>

This unified graph representation links visual features, textual semantics, and topological relationships, supporting spatially-aware multimodal learning beyond conventional image-based methods.

#### 3.2 Graph-based Data Structure

We conceptualize the pedestrian network as a spatial graph  $G = (V, E)$  where nodes  $V$  represent street intersections and edges  $E$  represent street segments. It provides both structural clarity for dataset navigation and foundations for future GNN applications. It comprises 208 locations organized into four types (Table 3):

**Nodes** ( $|V_{node}| = 81$ ): Street intersections encoded as "N- $i$ - $j$ " where  $i$  and  $j$  indicate row and column positions in the spatial grid. Nodes are classified by accessibility depth based on shortest-path distance to public roads [61].

**Edges - Streets** ( $|V_{edge}| = 125$ ): Pedestrian street segments connecting two nodes. Horizontal edges ( $|V_h| = 61$ , east-west orientation) encoded as "Eh- $i$ - $j$ "; vertical edges ( $|V_v| = 64$ , north-south orientation) as "Ev- $j$ - $i$ ". Each edge is characterized by physical attributes (length  $l_{ij}$ , width  $w_{ij}$ , orientation  $\theta_{ij}$ ). Streets are classified by width: Type 1 (1–3m), Type 2 (4–7m), Type 3 (8–13m) [28].

**Squares** ( $|V_{square}| = 2$ ): Large open spaces forming sub-graphs bounded by multiple edges and nodes, encoded as "S- $k$ " (ranked by area) and defined as  $S_k = (E_k, V_k)$  where  $E_k \subset E$  and  $V_k \subset V$  are the bounding edges and nodes respectively. The central square S-1 (area 2,347m<sup>2</sup>) serves as the primary gathering space.

This hierarchical encoding preserves both geometric position and topological relationships, enabling construction of adjacency matrices and distance metrics for graph-based learning algorithms.

### 3.3 Bridging Urban Design Theory with VPR

Traditional VPR datasets provide only visual appearance and coordinates, overlooking spatial configuration context that shapes human navigation [38, 61, 78]. Current VPR approaches face limitations: treating locations as isolated entities without relational context, struggling with non-uniform query distributions, and lacking support for context-aware queries. We integrate *space syntax* theory [36, 37] to enrich annotations with spatial configuration metrics, enabling: (1) topological context modeling; (2) flow-aware retrieval; (3) hierarchical search; (4) cross-city transfer.

**Metric Computation.** Space syntax comprises two main metrics: integration and betweenness. For each street  $i$  in the network of  $k$  streets, we compute *integration* (global accessibility, higher values indicate centrally-located, easily accessible streets):

$$\text{Integration}_i = \frac{k-2}{2\left(\frac{1}{k-1}\sum_{j \neq i} d(i,j) - 1\right)} \quad (1)$$

where  $d(i, j)$  is the shortest path distance.

*Betweenness* measures through-movement potential [36, 37] (higher values indicating primary routes with heavier pedestrian flow):

$$\text{Betweenness}_i = \sum_{\substack{j \neq i \\ k \neq i, k \neq j}} \frac{\sigma_{jk}(i)}{\sigma_{jk}} \quad (2)$$

where  $\sigma_{jk}(i)$  counts shortest paths passing through street  $i$ .

We employ both *angular distance*  $d_a = \sum_{turns} \theta_{turn}/90$  ([78]) and *weighted distance*  $d_w = 0.5 \cdot \text{norm}(d_e) + 0.5 \cdot \text{norm}(d_a)$  for distance definition, yielding four properties per street.

By integrating theoretically-grounded metrics from city science, we bridge urban analysis with VPR research, providing a richer semantic foundation for spatially-aware place recognition systems. While our current benchmark experiments primarily utilize visual and semantic text features, we provide space syntax annotations to facilitate future VPR research exploring synergies between visual appearance, semantic content, and spatial configuration.

## 4 Multimodal Street-level VPR Library: MMS-VPRLib

Recently, exploration of VPR methods has drawn great attention. Given the development of current methods, the issue of fair benchmarking poses great challenges for future research. In view of increasing demand for VPR benchmarks, VPR-Bench [89] and VPR-Ensem [26] have been proposed. However, these benchmarks have limitations. One issue is their failure to address multi-modal settings and incorporate state-of-the-art methods. Another limitation is the inability to utilize new architectures like Transformers or GNNs, as Table 1 shows. To address these limitations, we propose *MMS-VPRLib*, a benchmark designed for fair evaluation of VPR tasks across numerous multi-modal visual place recognition models as well as aggregation of unimodal models, as Figure 3 illustrates.

**Data Format.** MMS-VPRLib supports multi-modal inputs with different formats, like "png", "jpeg", "txt", "mp4", etc, as shown in Figure 3. MMS-VPRLib currently supports more than 10 datasets, covering areas from campus and shopping malls to city scenes. Beyond unimodality with just images, newly input multimodality is also supported, like MMS-VPR.

**Data Pre-processing.** Data pre-processing includes data cleaning, modality-specific normalisation (e.g., resizing/cropping and intensity scaling), and a principled training-validation-test split. For multimodal data, images/videos require frame sampling and visual normalisation (optionally with denoising/augmentation), while text requires normalisation, tokenisation and vocabulary filtering.

**Model Design.** We group the MMS-VPR models into two broad categories: (i) *unimodal* designs, which adopt modality-specific backbones together with explicit signal enhancement, alignment, and fusion components; and (ii) *multimodal* designs, which leverage end-to-end vision-language pre-training for unified representation learning. For visual inputs (images and video frames), we provide strong CNN and Transformer-based encoders (e.g., ResNet and ViT), with temporal aggregation and sequence modelling for videos (e.g., RNN/Transformer-style components) [25, 34, 80]. For text, we include both classical baselines (e.g., Word2Vec features with Random Forest classifiers) and pre-trained Transformer language models (e.g., BERT and XLNet; optionally GPT-style LMs where appropriate) [11, 24, 53, 67, 85]. For multimodal learning, we incorporate representative state-of-the-art vision language models, including CLIP, SigLIP, and BLIP, to support principled image-text (and extensible video-text) modelling within a unified pipeline [47, 66, 90].

- **Shallow Modelling Baselines (ML).** These methods operate on fixed, pre-extracted representations and therefore provide a capacity-controlled reference point, helping to disentangle performance gains brought by representation learning from those due to the classifier itself. They are also computationally lightweight, offering a practical lower bound in terms of model complexity.
- **CNN-based Baselines.** CNN backbones prioritise locality and translation invariance, which can be advantageous for capturing texture cues and robust mid-level patterns under moderate viewpoint change. We include both a generic CNN encoder and a classical VPR aggregation pipeline to reflect widely adopted convolutional design choices.
- **Transformer-based Baselines.** Transformer architectures provide global receptive fields via attention, making them suitable for modelling long-range spatial dependencies and learning compact global descriptors for retrieval. We include a generic Transformer vision backbone as well as recent VPR-oriented Transformer/attention-based designs and descriptor learning frameworks to ensure the comparison reflects current unimodal state-of-the-art practice.
- **Multimodal Modelling Baselines (Vision-Language Pre-training).** Vision-language foundation models provide strong transferable representations learned from large-scale multimodal corpora. Including such models enables assessment of whether cross-modal pre-training yields systematic gains under appearance, viewpoint, and environmental changes, and provides a competitive reference for multimodal feature extractors in our setting.

**Signal Enhancement.** MMS-VPRLib also introduces a dedicated signal enhancement module, serving as a robustness layer that restores and standardises multimodal inputs (e.g., low-light correction, deblurring/denoising, stabilisation, and text normalisation) prior to

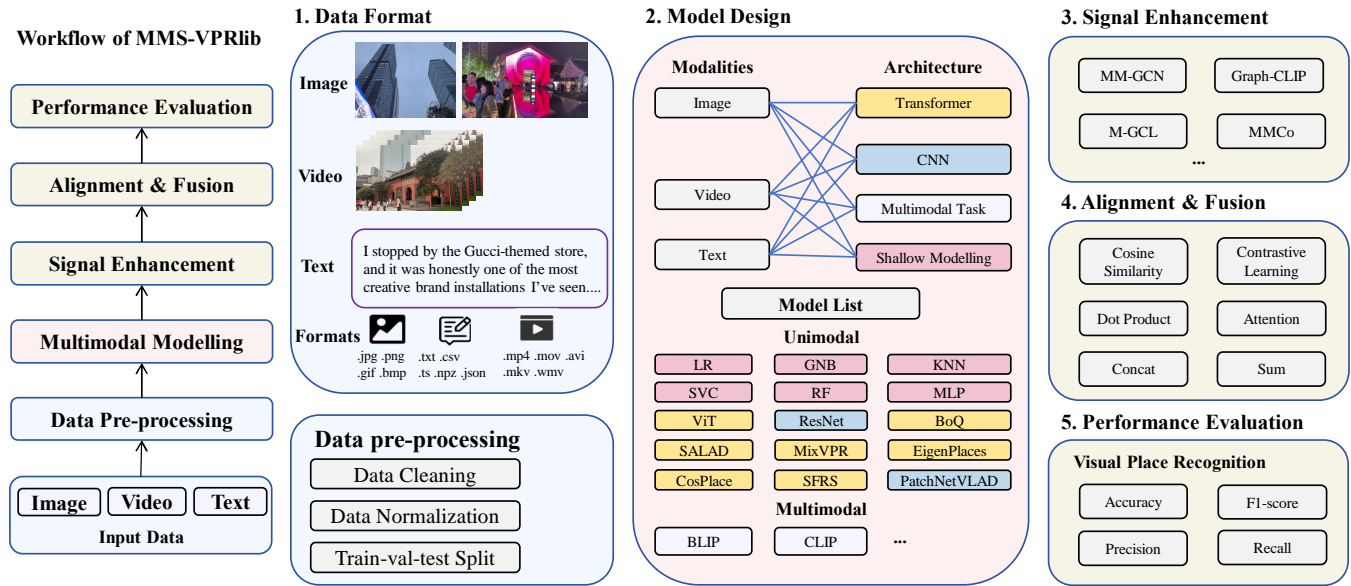


Figure 3: Workflow of Multi-modal Street-level Visual Place Recognition Benchmark.

alignment and fusion modules. By mitigating appearance degradations and modality-specific noise, it reduces spurious dataset biases, improves generalisation, and enables more faithful, reproducible comparisons across architectures and fusion strategies.

**Alignment, Fusion and Evaluation.** Alignment maps heterogeneous inputs (images, videos, and text) into a shared embedding space and enforces consistent query-reference association (including temporal/instance-level matching for video-text pairs and feature normalisation across encoders). On top of aligned representations, the platform supports both score-level and feature-level fusion, including cosine similarity or dot-product scoring per modality with aggregation, as well as embedding concatenation followed by optional projection for dimensionality control. Evaluation is standardised to ensure fair comparison across datasets and architectures: performance is reported with Recall@K, accuracy, F1-score, and precision. This integrated design makes multimodal gains traceable to specific alignment/fusion choices and supports reproducible, extensive benchmarking.

**Supported Datasets.** MMS-VPRlib supports a diverse set of current VPR datasets, spanning dense urban street scenes (e.g., Tokyo 24/7 [76], Pittsburgh [77], Cambridge [43], and CityPlace [21]) and other route-based scenarios, including campus-scale pedestrian navigation (New College [74]) and railway journeys with pronounced seasonal change (Nordland [75]). By unifying data loading and evaluation protocols across these benchmarks, it enables fair cross-dataset comparison and more systematic robustness assessment.

## 5 Experiment

### 5.1 Research Questions

In this section, we aim to answer the following questions:

- **RQ1:** Can MMS-VPRlib serve as a benchmark for multimodal VPR, particularly on MMS-VPR (image-video-text)? – Overall performance on MMS-VPR dataset
- **RQ2:** Can MMS-VPRlib support commonly used VPR datasets and produce reasonable results with widely used models? – Overall performance on unimodal dataset
- **RQ3:** How do the selected baselines differ in training/testing runtime and peak RAM, and how should these time-memory costs guide model choice under different performance targets? – Efficiency comparison
- **RQ4:** How sensitive is MMS-VPR performance to key hyperparameters and settings? – Sensitivity studies

### 5.2 Experiment Setup

**Baselines.** To ensure a fair and comprehensive comparison, we benchmark our method against baselines that span (i) classical shallow modelling baselines, (ii) CNN-based models, (iii) Transformer-based models, and (iv) Multimodal modelling baselines.

- **Shallow ML:** LR [39], GNB [52], SVC [19], KNN [20], RF [12], MLP [68].
- **CNN-based:** ResNet [35], PatchNetVLAD [32].
- **Transformer-based:** ViT [29], R2Former [92], SALAD [42], BoQ [3], CosPlace [9], MixVPR [2], EigenPlaces [10].
- **Multimodal:** CLIP [66], BLIP [47].

**Hyper Parameters.** We set the batch size of 16 and 64 for BLIP [47] and LR [39], respectively. We set 32 for other methods. The dropout rate is set to 0.2 for SFRS [27], 0.3 for Patch-NetVLAD [32], 0.6 for GAT [81], and 0.1 for other models. For SVC [19], RF [12], MLP [68], and GNB [52], we set the PCA dimensionality to 128. For BoQ [3] and SALAD [42], we freeze the pretrained backbone for 2 epochs. Other settings are shown in Table 5 in Appendix A.1.

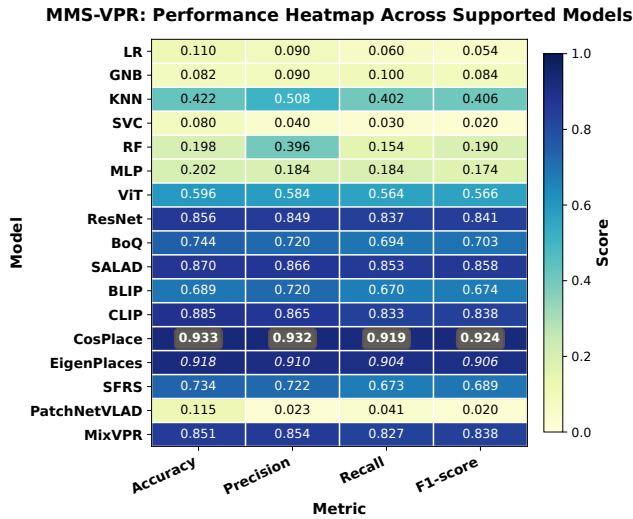


Figure 4: Model performances on MMS-VPR dataset. Results are reported as mean values (three decimal places).

### 5.3 RQ1: Results on multimodal datasets

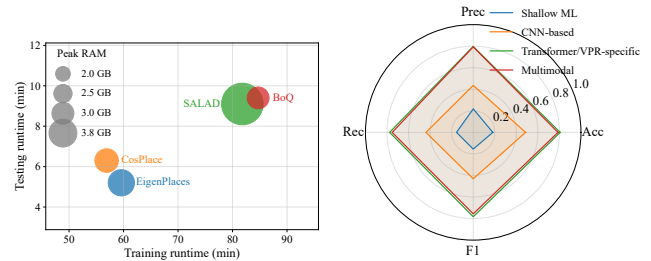
Figure 4 shows that the VPR-specialised baseline CosPlace achieves the strongest overall performance (*Accuracy*:0.933; *F1*:0.924). Relative to the strongest standard vision backbone, ResNet [35] (*Accuracy*:0.856; *F1*:0.841), CosPlace [9] yields a clear improvement of 9.0% in accuracy (0.856→0.933) and 9.9% in F1 (0.841→0.924). This suggests that VPR-oriented aggregation and metric-learning objectives provide additional gains beyond generic visual feature extraction.

Meanwhile, Transformer-based pretrained baselines remain competitive, but they still fall short of the top VPR pipeline. In particular, CLIP [66] shows a 5.1% lower accuracy than CosPlace [9] (0.933→0.885), and SALAD [42] is 6.8% lower (0.933→0.870). Nevertheless, pretraining offers substantial benefits over a plain transformer baseline: compared with ViT [29] (*Accuracy*: 0.596), CLIP improves accuracy by 48.5% (0.596→0.885), highlighting the practical value of large-scale pre-training even though specialised VPR designs remain the best-performing option in this setting.

Overall, MMS-VPRlib advances beyond VPR-Bench [89] by incorporating state-of-the-art Transformer-based and multimodal methods, enabling a more rigorous, comprehensive and representative assessment of modern multimodal VPR performance.

### 5.4 RQ2: Results on unimodal datasets

Table 4 reports unimodal performance across five datasets (Tokyo, New College, Pitt, Nordland, and Cambridge). Overall, BoQ [3] achieves the strongest and most consistent results, ranking first on Tokyo (Acc: 0.975), joint-first on Pitt (Acc: 0.920), and showing competitive performance on Nordland (Acc: 0.817) and Cambridge (Acc: 0.984). SALAD [42] provides the second-best overall performance, particularly excelling on New College (Acc: 0.844) and Cambridge (Acc: 0.987), while maintaining strong results on Nordland (Acc: 0.744). Among the remaining baselines, EigenPlaces [10] yields strong results on Tokyo (Acc: 0.927) and Pitt (Acc: 0.920), showing robust city-scale retrieval capabilities. Conventional VPR pipelines



(a) Runtime-memory cost (bubble area  $\propto$  peak RAM). (b) Category-level performance (mean over models).

Figure 5: Efficiency and performances on MMS-VPR.

(e.g., Patch-NetVLAD) underperform markedly on city-scale retrieval benchmarks (Tokyo/New College/Pitt), yet remain more competitive on sequence-style datasets, especially Nordland (Acc: 0.430) and structured indoor environments like Cambridge (Acc: 0.569). Lightweight vision backbones (ResNet [35], ViT [29]) and other VPR aggregation methods (MixVPR [2], CosPlace [9]) form a mid-tier group, with clear gains on Nordland and Cambridge but limited robustness across all city datasets.

To sum up, MMS-VPRlib successfully supports commonly used VPR datasets and produces reasonable results with widely used models. The platform’s standardized pipeline enables fair comparison across diverse benchmarks, with Transformer-based and multimodal approaches (BoQ, SALAD, EigenPlaces) consistently outperforming traditional CNN baselines across most scenarios. This demonstrates the library’s capability as a unified evaluation framework for the VPR community.

### 5.5 RQ3: Running time and memory

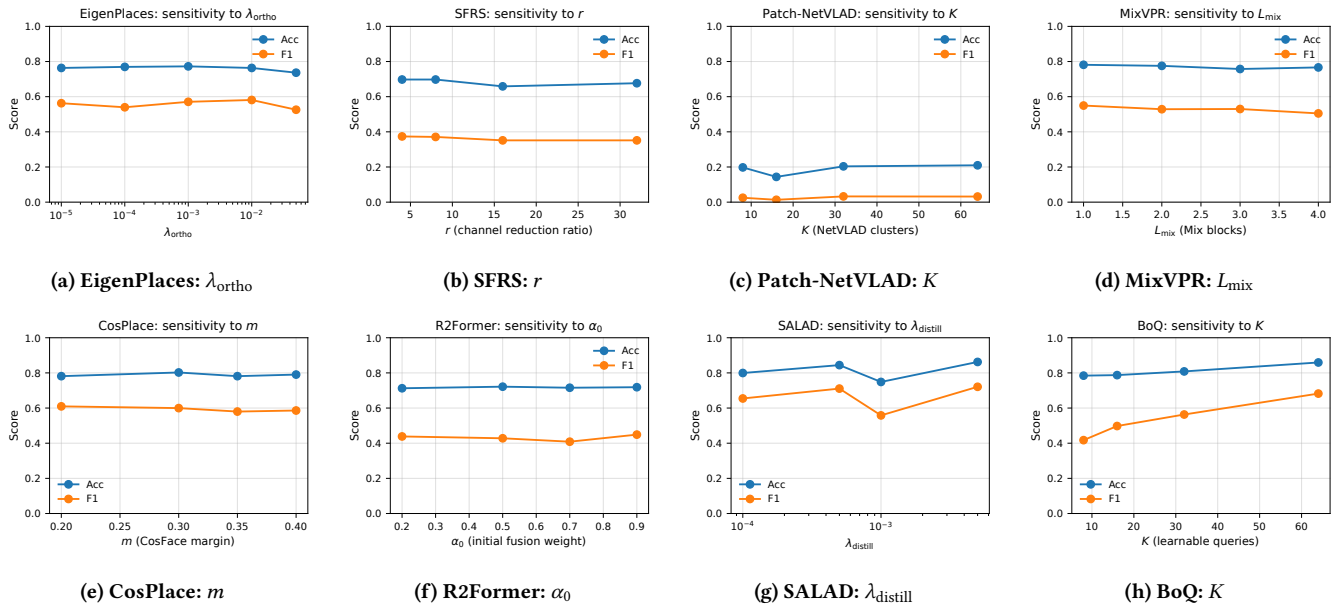
To facilitate practical model selection under realistic compute constraints, Figure 5 jointly characterises the efficiency and performance profiles of baselines. The runtime-memory plot (Figure 5a) indicates that CosPlace [9] and EigenPlaces [10] achieve strong accuracy with relatively modest runtime and peak RAM, making them suitable defaults when throughput and hardware budgets are limited, whereas SALAD [42] incurs the highest memory cost (3.8 GB), increasing deployment requirements. Complementarily, the category-mean radar plot (Figure 5b) shows that Transformer/VPR-specific methods dominate performance across Accuracy, Precision, Recall, and F1, while shallow ML and CNN baselines lag behind, highlighting the common trade-off between higher accuracy and greater computational demand.

### 5.6 RQ4: Sensitivity studies

We provide sensitivity studies in Figure 6 to identify robust operating ranges for fair comparison and reproducible deployment. Overall, performance exhibits clear hyperparameter-dependent regimes. EigenPlaces is relatively stable for  $\lambda_{ortho} \in [10^{-3}, 10^{-2}]$ , while SFRS [27] favours mild channel reduction ( $r = 4-8$ ). PatchNetVLAD [32] remains weak, with only marginal gains at  $K = 32-64$ . MixVPR [2] performs best with a shallow design ( $L_{mix} = 1$ ). CosPlace [9] prefers smaller margins ( $m \approx 0.2-0.3$ ). R2Former [92]

**Table 4: Performance comparison across five selected datasets. Best and second-best baselines in each column are highlighted in bold and underlined, respectively. Rows are ordered from lower to higher overall accuracy (better models appear lower).**

Model	Tokyo				New College				Pitt				Nordland				Cambridge			
	Acc	P	R	F1																
PatchNetVLAD [32]	0.846	0.838	0.860	0.845	0.144	0.009	0.038	0.013	0.870	0.860	0.887	0.860	0.430	0.420	0.449	0.410	0.569	0.207	0.321	0.250
R2Former [92]	0.771	0.775	0.770	0.765	0.722	0.453	0.429	0.428	0.910	0.910	0.911	0.910	0.710	0.710	0.720	0.710	0.946	0.943	0.923	0.932
ViT [29]	0.606	0.602	0.612	0.599	0.641	0.447	0.484	0.452	0.701	0.698	0.712	0.701	0.523	0.521	0.531	0.522	0.815	0.764	0.752	0.756
SFRS [27]	0.579	0.583	0.585	0.576	0.659	0.355	0.362	0.352	0.880	0.880	0.891	0.880	0.150	0.150	0.160	0.150	0.959	0.934	0.929	0.931
BLIP [47]	0.674	0.678	0.683	0.671	0.686	0.527	0.477	0.480	0.761	0.772	0.782	0.771	0.583	0.592	0.603	0.592	0.818	0.793	0.714	0.739
MixVPR [2]	0.789	0.793	0.785	0.781	0.758	0.549	0.533	0.530	0.904	0.912	0.915	0.917	0.730	0.730	0.762	0.730	0.974	0.971	0.959	0.965
EigenPlaces [10]	0.927	0.929	0.930	0.921	0.773	0.587	0.583	0.571	<b>0.920</b>	<b>0.920</b>	<b>0.925</b>	<b>0.920</b>	0.681	0.689	0.712	0.694	0.968	0.954	0.951	0.953
ResNet [35]	0.794	0.798	0.801	0.790	0.775	<u>0.633</u>	<u>0.618</u>	<u>0.611</u>	0.879	0.881	0.889	0.879	<b>0.861</b>	<b>0.830</b>	<u>0.814</u>	<u>0.815</u>	0.968	0.963	0.958	0.959
CosPlace [9]	0.816	0.819	0.822	0.812	0.781	0.588	0.596	0.580	0.900	0.900	0.909	0.900	0.560	0.560	0.585	0.560	0.974	0.977	0.953	0.964
CLIP [66]	0.843	0.846	0.851	0.839	<u>0.790</u>	0.500	0.529	0.503	0.901	0.899	0.903	0.897	0.742	0.741	0.753	0.742	0.930	0.931	0.914	0.917
BoQ [3]	<b>0.975</b>	<b>0.977</b>	<b>0.981</b>	<b>0.973</b>	<b>0.787</b>	0.494	0.533	0.498	<u>0.920</u>	<u>0.920</u>	<u>0.924</u>	<u>0.920</u>	<u>0.817</u>	<u>0.821</u>	<b>0.831</b>	<b>0.826</b>	<u>0.984</u>	<u>0.976</u>	<u>0.973</u>	<u>0.974</u>
SALAD [42]	0.804	0.807	0.800	0.795	<b>0.844</b>	<b>0.711</b>	<b>0.724</b>	<b>0.711</b>	0.611	0.644	0.621	0.627	0.744	0.727	0.763	0.709	<b>0.987</b>	<b>0.985</b>	<b>0.987</b>	<b>0.986</b>

**Figure 6: Sensitivity analysis across representative VPR models. Each subplot shows Acc and F1 versus a key hyperparameter.**

shows limited sensitivity to  $\alpha_0$ . SALAD [42] benefits from stronger distillation (best at  $\lambda_{distill} = 5 \times 10^{-3}$ ), and BoQ [3] improves with more queries, peaking at  $K = 64$ .

To sum up, MMS-VPRLib baselines exhibit relatively robust performance across typical hyperparameter ranges. These findings provide clear operating guidelines for reproducible deployment and fair comparison across different VPR methods, confirming the robustness of the MMS-VPRLib platform.

## 6 Conclusion

In this paper, we present **MMS-VPR**, a fine-grained, richly annotated, and structurally organized benchmark designed for pedestrian-centric urban environments. Unlike existing datasets dominated by vehicle-mounted imagery and large-scale road networks, MMS-VPR captures diverse urban scenes—such as commercial streets and public squares—from multiple viewpoints, times of day, and modalities including images, videos, textual descriptions, and geospatial

metadata. By modeling urban layouts as node–edge graphs, our dataset supports structural reasoning via graph neural networks, capturing the topological features and semantic relationships inherent in urban street layouts, which complements traditional visual and multimodal approaches.

To further support benchmarking and model development, we introduce **MMS-VPRLib**, a lightweight and extensible library that facilitates multimodal fusion and evaluation across diverse backbone models. MMS-VPRLib is designed to leverage the MMS-VPR dataset for end-to-end VPR tasks, and also serves as a toolkit for assessing the impact of multimodal inputs on existing VPR models. Extensive experiments across visual and multimodal models validate both the quality of MMS-VPR and the effectiveness of integrating heterogeneous inputs for place recognition. Our low-cost, smartphone-based data collection framework lowers the barrier for VPR dataset creation, supporting broader multimodal VPR research while enabling dataset construction in diverse global contexts.

## References

- [1] Amar Ali-bey, Brahim Chaib-draa, and Philippe Giguère. 2022. GSV-Cities: Toward appropriate supervised visual place recognition. *Neurocomputing* 513 (2022), 194–203. doi:10.1016/j.neucom.2022.09.127
- [2] Amar Ali-bey, Brahim Chaib-draa, and Philippe Giguère. 2023. MixVPR: Feature Mixing for Visual Place Recognition. In *Proceedings of the IEEE/CVF Winter Conference on Applications of Computer Vision*. 2998–3007.
- [3] Amar Ali-Bey, Brahim Chaib-draa, and Philippe Giguère. 2024. BoQ: A Place is Worth a Bag of Learnable Queries. arXiv:2405.07364 [cs.CV] <https://arxiv.org/abs/2405.07364>
- [4] Dragomir Anguelov, Carole Dulong, Daniel Filip, Christian Frueh, Stéphane Lafon, Richard Lyon, Abhijit Ogale, Luc Vincent, and Josh Weaver. 2010. Google street view: Capturing the world at street level. *Computer* 43, 6 (2010), 32–38.
- [5] Asha Anooosheh, Torsten Sattler, Radu Timofte, Marc Pollefeys, and Luc Van Gool. 2019. Night-to-day image translation for retrieval-based localization. In *IEEE International Conference on Robotics and Automation (ICRA)*. IEEE, 5958–5964.
- [6] Apple Inc. 2019. iPhone 11 Pro Technical Specifications. <https://support.apple.com/kb/SP805>. Accessed: 2024-10-15.
- [7] Gabriele Berton, Lorenz Junglas, Riccardo Zaccone, Thomas Pollok, Barbara Caputo, and Carlo Masone. 2024. MeshVPR: Citywide Visual Place Recognition Using 3D Meshes. In *European Conference on Computer Vision*. Springer, 321–339.
- [8] Gabriele Berton, Carlo Masone, and Barbara Caputo. 2022. Rethinking visual geo-localization for large-scale applications. *IEEE Conference on Computer Vision and Pattern Recognition* (2022), 4878–4888.
- [9] Gabriele Berton, Carlo Masone, and Barbara Caputo. 2022. Rethinking Visual Geo-Localization for Large-Scale Applications. In *Proceedings of the IEEE/CVF Conference on Computer Vision and Pattern Recognition (CVPR)*. 4878–4888.
- [10] Gabriele Berton, Gabriele Trivigno, Barbara Caputo, and Carlo Masone. 2023. EigenPlaces: Training Viewpoint Robust Models for Visual Place Recognition. In *Proceedings of the IEEE/CVF International Conference on Computer Vision (ICCV)*. 11080–11090.
- [11] Leo Breiman. 2001. Random Forests. *Machine Learning* 45, 1 (2001), 5–32. doi:10.1023/A:1010933404324
- [12] Leo Breiman. 2001. Random Forests. *Machine Learning* 45 (2001), 5–32.
- [13] Leonardo Brizi, Emanuele Giacomini, Luca Di Giammarino, Simone Ferrari, Omar Salem, Lorenzo De Rebotti, and Giorgio Grisetti. 2024. VBR: a vision benchmark in Rome. In *2024 IEEE International Conference on Robotics and Automation (ICRA)*. IEEE, 15868–15874.
- [14] Nicholas Carlevaris-Bianco, Arash K Ushani, and Ryan M Eustice. 2016. University of Michigan North Campus long-term vision and lidar dataset. *The International Journal of Robotics Research* 35, 9 (2016), 1023–1035.
- [15] Nicholas Carlevaris-Bianco, Arash K. Ushani, and Ryan M. Eustice. 2016. University of Michigan North Campus long-term vision and lidar dataset. *Int. J. Robotics Res.* 35 (2016), 1023–1035. doi:10.1177/0278364915614638
- [16] Mathilde Caron, Hugo Touvron, Ishan Misra, Hervé Jégou, Julien Mairal, Piotr Bojanowski, and Armand Joulin. 2021. Emerging properties in self-supervised vision transformers. In *Proceedings of the IEEE/CVF International Conference on Computer Vision*. 9650–9660.
- [17] David M Chen, Georges Baatz, Kevin Köser, Sam S Tsai, Ramakrishna Vedantham, Timo Pylvänäinen, Kimmo Roimela, Xin Chen, Jeff Bach, Marc Pollefeys, et al. 2011. City-scale landmark identification on mobile devices. In *CVPR 2011*. IEEE, 737–744.
- [18] David M. Chen, Georges Baatz, Kevin Köser, Sam S. Tsai, Ramakrishna Vedantham, Timo Pylvänäinen, Kimmo Roimela, Xin Chen, Jeff Bach, Marc Pollefeys, Bernd Girod, and Radek Grzeszczuk. 2011. City-scale landmark identification on mobile devices. In *Proceedings of the 24th IEEE Conference on Computer Vision and Pattern Recognition (CVPR)*. IEEE Computer Society, 737–744. doi:10.1109/CVPR.2011.5995610
- [19] Corinna Cortes and Vladimir Vapnik. 1995. Support-Vector Networks. In *Machine Learning*, Vol. 20. 273–297.
- [20] Thomas Cover and Peter Hart. 1967. Nearest Neighbor Pattern Classification. In *IEEE Transactions on Information Theory*, Vol. 13. 21–27.
- [21] Mark Cummins and Paul Newman. 2008. FAB-MAP: Probabilistic Localization and Mapping in the Space of Appearance. *The International Journal of Robotics Research* 27, 6 (2008), 647–665. doi:10.1177/0278364908090961
- [22] James E Cutting and Peter M Vishton. 2002. Reconciling perceptual space. *Perception of space and motion* (2002), 215–234.
- [23] Jia Deng, Wei Dong, Richard Socher, Li-Jia Li, Kai Li, and Li Fei-Fei. 2009. Imagenet: A large-scale hierarchical image database. *IEEE Conference on Computer Vision and Pattern Recognition* (2009), 248–255.
- [24] Jacob Devlin, Ming-Wei Chang, Kenton Lee, and Kristina Toutanova. 2019. Bert: Pre-training of deep bidirectional transformers for language understanding. In *Proceedings of the 2019 conference of the North American chapter of the association for computational linguistics: human language technologies, volume 1 (long and short papers)*. 4171–4186.
- [25] Alexey Dosovitskiy, Lucas Beyer, Alexander Kolesnikov, Dirk Weissenborn, Xiuhua Zhai, Thomas Unterthiner, Mostafa Dehghani, Matthias Minderer, Georg Heigold, Sylvain Gelly, Jakob Uszkoreit, and Neil Houlsby. 2021. An Image is Worth 16x16 Words: Transformers for Image Recognition at Scale. In *International Conference on Learning Representations (ICLR)*.
- [26] Tobias Fischer, Matthew Xu, Saumya Jain, and Michael Milford. 2025. Ensemble-Based Event Camera Place Recognition Under Varying Illumination. *IEEE Robotics and Automation Letters* (2025). doi:10.1109/LRA.2025.3641119
- [27] Yixiao Ge, Haibo Wang, Feng Zhu, Rui Zhao, and Hongsheng Li. 2020. Self-supervising Fine-Grained Region Similarities for Large-Scale Image Localization. In *Computer Vision – ECCV 2020*, Andrea Vedaldi, Horst Bischof, Thomas Brox, and Jan-Michael Frahm (Eds.), 369–386.
- [28] Jan Gehl. 2011. *Life Between Buildings: Using Public Space* (6th ed.). Island Press, Washington, DC.
- [29] Kai Han, Yunhe Wang, Hanqing Chen, Xinghao Chen, Jianyuan Guo, Zhenhua Liu, Yehui Tang, An Xiao, Chunqing Xu, Yixing Xu, et al. 2022. A survey on vision transformer. *IEEE transactions on pattern analysis and machine intelligence* 45, 1 (2022), 87–110.
- [30] Rifat Hasan, SM Nahid Hasan, Anika Tasnim Islam, and Fauzia Yasmeen. 2023. Customer Review Generation in a Shopping Mall Using Sentiment Analysis and Computer Vision. *Journal of Far East International University* 6, 1 (2023), 39–48.
- [31] Daniel Cabrini Hauage and Noah Snavely. 2012. Image matching using local symmetry features. In *IEEE Conference on Computer Vision and Pattern Recognition (CVPR)*. IEEE, 206–213.
- [32] Stephen Hausler, Sourav Garg, Ming Xu, Michael Milford, and Tobias Fischer. 2021. Patch-NetVLAD: Multi-Scale Fusion of Locally-Global Descriptors for Place Recognition. In *Proceedings of the IEEE/CVF Conference on Computer Vision and Pattern Recognition*. 14141–14152.
- [33] James Hays and Alexei A Efros. 2008. IM2GPS: estimating geographic information from a single image. In *IEEE Conference on Computer Vision and Pattern Recognition (CVPR)*. IEEE, 1–8.
- [34] Kaiming He, Xiangyu Zhang, Shaoqing Ren, and Jian Sun. 2016. Deep Residual Learning for Image Recognition. In *Proceedings of the IEEE Conference on Computer Vision and Pattern Recognition (CVPR)*. 770–778.
- [35] Kaiming He, Xiangyu Zhang, Shaoqing Ren, and Jian Sun. 2016. Deep residual learning for image recognition. In *Proceedings of the IEEE conference on computer vision and pattern recognition*. 770–778.
- [36] Bill Hillier. 1996. *Space is the Machine: A Configurational Theory of Architecture*. Cambridge University Press, Cambridge, UK.
- [37] Bill Hillier and Julienne Hanson. 1984. *The Social Logic of Space*. Cambridge University Press, Cambridge, UK.
- [38] Bill Hillier, Alan Penn, Julienne Hanson, Tadeusz Grajewski, and Jianming Xu. 1993. Natural movement: or, configuration and attraction in urban pedestrian movement. *Environment and Planning B: Planning and Design* 20, 1 (1993), 29–66.
- [39] David W. Hosmer, Stanley Lemeshow, and Rodney X. Sturdivant. 2013. *Applied Logistic Regression*. Wiley.
- [40] Gaoshuang Huang, Yang Zhou, Xiaofei Hu, Chenglong Zhang, Luying Zhao, and Wenjian Gan. 2024. DINO-Mix enhancing visual place recognition with foundational vision model and feature mixing. *Scientific Reports* 14, 1 (2024), 22100.
- [41] Gaoshuang Huang, Yang Zhou, Luying Zhao, and Wenjian Gan. 2025. CV-Cities: Advancing Cross-View Geo-Localization in Global Cities. *IEEE J. Sel. Top. Appl. Earth Obs. Remote. Sens.* 18 (2025). doi:10.1109/JSTARS.2024.3502160
- [42] Sergio Izquierdo and Javier Civera. 2024. Optimal Transport Aggregation for Visual Place Recognition. In *Proceedings of the IEEE/CVF Conference on Computer Vision and Pattern Recognition (CVPR)*.
- [43] Alex Kendall, Matthew Grimes, and Roberto Cipolla. 2015. PoseNet: A Convolutional Network for Real-Time 6-DOF Camera Relocalization. In *Proceedings of the IEEE International Conference on Computer Vision (ICCV)*. 2938–2946.
- [44] Giseop Kim, Yeong Sang Park, Younghun Cho, Jinyong Jeong, and Ayoung Kim. 2020. Mulran: Multimodal range dataset for urban place recognition. In *2020 IEEE international conference on robotics and automation (ICRA)*. IEEE, 6246–6253.
- [45] Donghwan Lee, Soohyun Ryu, Suyong Yeon, Yonghan Lee, Deokhwa Kim, Cheolho Han, Johann Cabon, Philippe Weinzaepfel, Nicolas Guérin, Gabriela Csurka, et al. 2021. Large-scale localization datasets in crowded indoor spaces. In *Proceedings of the IEEE/CVF Conference on Computer Vision and Pattern Recognition*. 3227–3236.
- [46] Donghwan Lee, Soo-Hyun Ryu, Suyong Yeon, Yonghan Lee, Deokhwa Kim, Cheolho Han, Johann Cabon, Philippe Weinzaepfel, Nicolas Guérin, Gabriela Csurka, and Martin Humenberger. 2021. Large-Scale Localization Datasets in Crowded Indoor Spaces. In *Proceedings of the IEEE/CVF Conference on Computer Vision and Pattern Recognition (CVPR)*. IEEE / Computer Vision Foundation, 3227–3236. doi:10.1109/CVPR46437.2021.00324
- [47] Junnan Li, Dongxu Li, Caiming Xiong, and Steven C. H. Hoi. 2022. BLIP: Bootstrapping Language-Image Pre-training for Unified Vision-Language Understanding and Generation. In *International Conference on Machine Learning (ICML)*. 12888–12900. <https://proceedings.mlr.press/v162/li22n.html>
- [48] Stephanie Lowry, Niko Sünderhauf, Paul Newman, John J Leonard, David Cox, Peter Corke, and Michael J Milford. 2015. Visual place recognition: A survey. *IEEE transactions on robotics* 32, 1 (2015), 1–19.

- [49] Stephanie Lowry, Niko Sünderhauf, Paul Newman, Will Maddern, Michael Milford, et al. 2016. Visual place recognition: A survey. *IEEE Transactions on Robotics* 32, 1 (2016), 1–19.
- [50] Zonglin Lyu, Juexiao Zhang, Mingxuan Lu, Yiming Li, and Chen Feng. 2024. Tell me where you are: Multimodal llms meet place recognition. *arXiv preprint arXiv:2406.17520* (2024).
- [51] Will Maddern, Geoffrey Pascoe, Chris Linegar, and Paul Newman. 2017. 1 year, 1000 km: The Oxford RobotCar dataset. *The International Journal of Robotics Research* 36, 1 (2017), 3–15.
- [52] Andrew McCallum and Kamal Nigam. 1998. A Comparison of Event Models for Naive Bayes Text Classification. In *AAAI-98 Workshop on Learning for Text Categorization*.
- [53] Tomáš Mikolov, Kai Chen, Greg Corrado, and Jeffrey Dean. 2013. Efficient Estimation of Word Representations in Vector Space. In *International Conference on Learning Representations (ICLR) Workshop Track*. <http://arxiv.org/abs/1301.3781>
- [54] Wenwen Ming, Xucan Chen, Zhe Liu, Ruihao Li, and Wei Yi. 2025. Hierarchical Visual Place Recognition with Semantic-Guided Attention. In *International Conference on Pattern Recognition*. Springer, 377–392.
- [55] Gerhard Neuhold, Tobias Ollmann, Samuel Rota Buló, and Peter Kontschieder. 2017. The Mapillary Vistas Dataset for Semantic Understanding of Street Scenes. In *Proceedings of the IEEE International Conference on Computer Vision (ICCV)*. IEEE Computer Society, 5000–5009. doi:10.1109/ICCV.2017.534
- [56] Gerhard Neuhold, Tobias Ollmann, Samuel Rota Buló, and Peter Kontschieder. 2017. The Mapillary Vistas dataset for semantic understanding of street scenes. In *IEEE International Conference on Computer Vision (ICCV)*. 4990–4999.
- [57] Stephen E Palmer. 1999. *Vision science: Photons to phenomenology*. MIT Press.
- [58] Taiyi Pan, Junyang He, Chao Chen, Yiming Li, and Chen Feng. 2024. NYC-Event-VPR: A Large-Scale High-Resolution Event-Based Visual Place Recognition Dataset in Dense Urban Environments. *arXiv preprint arXiv:2410.21615* (2024).
- [59] Taiyi Pan, Junyang He, Chao Chen, Yiming Li, and Chen Feng. 2024. NYC-Event-VPR: A Large-Scale High-Resolution Event-Based Visual Place Recognition Dataset in Dense Urban Environments. *arXiv preprint arXiv:2410.21615* (2024). Submitted on 28 Oct 2024.
- [60] Eleonora Pantano, Charles Dennis, and Michela De Pietro. 2021. Shopping centers revisited: the interplay between consumers' spontaneous online communications and retail planning. *Journal of Retailing and Consumer Services* 61 (2021), 102576.
- [61] John Peponis, Craig Zimring, and Yoon Kyung Choi. 1997. On the description of shape and spatial configuration inside buildings: convex partitions and their local properties. *Environment and Planning B: Planning and Design* 24, 5 (1997), 761–781.
- [62] Horia Porav, Will Maddern, and Paul Newman. 2018. Don't worry about the weather: Unsupervised condition-dependent domain adaptation. In *IEEE International Conference on Intelligent Transportation Systems (ITSC)*. IEEE, 33–40.
- [63] Yulia Preobrazhenskaya, Alton Chua, and Khasfariyati Razikin. 2019. Analysis of geotagged photos for understanding tourist temporal behavior. *Tourism Geographies* 21, 4 (2019), 631–656.
- [64] Minh-Duc Quach, Duc-Minh Vo, and Hoang-Anh Pham. 2024. MS-MixVPR: Multi-scale Feature Mixing Approach for Long-Term Place Recognition. *SN Computer Science* 5, 6 (2024), 656.
- [65] Alec Radford, Jong Wook Kim, Chris Hallacy, Aditya Ramesh, Gabriel Goh, Sandhini Agarwal, Girish Sastry, Amanda Askell, Pamela Mishkin, Jack Clark, et al. 2021. Learning transferable visual models from natural language supervision. In *International conference on machine learning*. PmlR, 8748–8763.
- [66] Alec Radford, Jong Wook Kim, Chris Hallacy, Aditya Ramesh, Gabriel Goh, Sandhini Agarwal, Girish Sastry, Amanda Askell, Pamela Mishkin, Jack Clark, Gretchen Krueger, and Ilya Sutskever. 2021. Learning Transferable Visual Models From Natural Language Supervision. In *International Conference on Machine Learning (ICML)*. 8748–8763. <https://proceedings.mlr.press/v139/radford21a.html>
- [67] Alec Radford, Jeff Wu, Rewon Child, David Luan, Dario Amodei, and Ilya Sutskever. 2019. Language Models are Unsupervised Multitask Learners. (2019). [https://cdn.openai.com/better-language-models/language\\_models\\_are\\_unsupervised\\_multitask\\_learners.pdf](https://cdn.openai.com/better-language-models/language_models_are_unsupervised_multitask_learners.pdf)
- [68] David E. Rumelhart, Geoffrey E. Hinton, and Ronald J. Williams. 1986. Learning representations by back-propagating errors. In *Nature*, Vol. 323. 533–536.
- [69] Mark S Sanders and Ernest J McCormick. 1993. *Human factors in engineering and design* (7th ed.). McGraw-Hill.
- [70] Torsten Sattler, Will Maddern, Carl Toft, Akihiko Torii, Lars Hammarstrand, Erik Stenborg, Daniel Safari, Masatoshi Okutomi, Marc Pollefeys, Josef Sivic, et al. 2018. Benchmarking 6DOF outdoor visual localization in changing conditions. In *IEEE Conference on Computer Vision and Pattern Recognition (CVPR)*. 8601–8610.
- [71] Diwei Sheng, Yuxiang Chai, Xinru Li, Chen Feng, Jianzhe Lin, Claudio Silva, and John-Ross Rizzo. 2021. NYU-VPR: Long-term visual place recognition benchmark with view direction and data anonymization influences. In *2021 IEEE/RSJ International Conference on Intelligent Robots and Systems (IROS)*. IEEE, 9773–9779.
- [72] Diwei Sheng, Yuxiang Chai, Xinru Li, Chen Feng, Jianzhe Lin, Cláudio T. Silva, and John-Ross Rizzo. 2021. NYU-VPR: Long-Term Visual Place Recognition Benchmark with View Direction and Data Anonymization Influences. In *Proceedings of the IEEE/RSJ International Conference on Intelligent Robots and Systems (IROS)*. IEEE, 9773–9779. doi:10.1109/IROS51168.2021.9636640
- [73] Tavis Shore, Oscar Mendez, and Simon Hadfield. 2025. SpaGBOL: Spatial-Graph-Based Orientated Localisation. In *Proceedings of the Winter Conference on Applications of Computer Vision (WACV)*. 6858–6867.
- [74] Mike Smith, Ian Baldwin, Winston Churchill, Rohan Paul, and Paul Newman. 2009. The New College Vision and Laser Data Set. *The International Journal of Robotics Research* 28, 5 (May 2009), 595–599.
- [75] Niko Sünderhauf, Peer Neubert, and Peter Protzel. 2013. Are We There Yet? Challenging SeqSLAM on a 3000 km Journey Across All Four Seasons. In *ICRA 2013 Workshop on Long-Term Autonomy*. Karlsruhe, Germany.
- [76] Akihiko Torii, Relja Arandjelović, Josef Sivic, Masatoshi Okutomi, and Tomáš Pajdla. 2018. 24/7 Place Recognition by View Synthesis. *IEEE Transactions on Pattern Analysis and Machine Intelligence* 40 (2018), 257–271. doi:10.1109/TPAMI.2017.2667665
- [77] Akihiko Torii, Josef Sivic, Masatoshi Okutomi, and Tomáš Pajdla. 2015. Visual Place Recognition with Repetitive Structures. *IEEE Transactions on Pattern Analysis and Machine Intelligence* 37, 11 (2015), 2346–2359. doi:10.1109/TPAMI.2015.2409868
- [78] Alasdair Turner, Maria Doxa, David O'Sullivan, and Alan Penn. 2001. From isovists to visibility graphs: a methodology for the analysis of architectural space. *Environment and Planning B: Planning and Design* 28, 1 (2001), 103–121.
- [79] Julien Valentin, Vibhav Vineet, Ming-Ming Cheng, David Kim, Jamie Shotton, Pushmeet Kohli, Matthias Niessner, Antonio Criminisi, Shahram Izadi, and Philip Torr. 2016. Learning to navigate the energy landscape. *IEEE Transactions on Pattern Analysis and Machine Intelligence* 38, 11 (2016), 2283–2296.
- [80] Ashish Vaswani, Noam Shazeer, Niki Parmar, Jakob Uszkoreit, Llion Jones, Aidan N. Gomez, Lukasz Kaiser, and Illia Polosukhin. 2017. Attention Is All You Need. In *Advances in Neural Information Processing Systems (NeurIPS)*.
- [81] Petar Veličković, Guillem Cucurull, Arantxa Casanova, Adriana Romero, Pietro Lio, and Yoshua Bengio. 2017. Graph attention networks. *arXiv preprint arXiv:1710.10903* (2017).
- [82] Changwei Wang, Shunpeng Chen, Yukun Song, Rongtao Xu, Zherui Zhang, Jiguang Zhang, Haoran Yang, Yu Zhang, Kexue Fu, Shide Du, et al. 2025. Focus on Local: Finding Reliable Discriminative Regions for Visual Place Recognition. In *Proceedings of the AAAI Conference on Artificial Intelligence*, Vol. 39. 7536–7544.
- [83] Frederik Warburg, Søren Hauberg, Manuel López-Antequera, Pau Gargallo, Yubin Kuang, and Javier Civera. 2020. Mapillary Street-Level Sequences: A Dataset for Lifelong Place Recognition. In *Proceedings of the IEEE/CVF Conference on Computer Vision and Pattern Recognition (CVPR)*. IEEE Computer Society / Computer Vision Foundation, 2623–2632. doi:10.1109/CVPR42606.2020.00270
- [84] Chenyu Wu, Shaoqi Hou, Zebang Qin, Guangqiang Yin, Xinzhong Wang, and Zhiguo Wang. 2024. Gicnet: global information capture network for visual place recognition. *Multimedia Systems* 30, 6 (2024), 337.
- [85] Zhilin Yang, Zihang Dai, Yiming Yang, Jaime G. Carbonell, Ruslan Salakhutdinov, and Quoc V. Le. 2019. XLNet: Generalized Autoregressive Pretraining for Language Understanding. In *Advances in Neural Information Processing Systems (NeurIPS)*. 5754–5764.
- [86] Shanshan Yi and Xiaofang Liu. 2020. Machine learning based customer sentiment analysis for recommending shoppers, shops based on customers' review. *Complex & Intelligent Systems* 6, 3 (2020), 621–634.
- [87] Burak Yildiz, Seyran Khademi, Ronald Maria Siebes, and Jan C. van Gemert. 2022. AmsterTime: A Visual Place Recognition Benchmark Dataset for Severe Domain Shift. In *Proceedings of the 26th International Conference on Pattern Recognition (ICPR)*. IEEE, 2749–2755. doi:10.1109/ICPR56361.2022.9956049
- [88] Dmitry A. Yudin, Yaroslav K. Solomentsev, Ruslan Musaev, Aleksei Staroverov, and Aleksandr I. Panov. 2022. HPointLoc: Point-Based Indoor Place Recognition Using Synthetic RGB-D Images. In *Neural Information Processing - 29th International Conference, ICONIP 2022, Virtual Event, November 22–26, 2022, Proceedings, Part III (Lecture Notes in Computer Science, Vol. 13625)*. Springer, 471–484. doi:10.1007/978-3-031-30111-7\_40
- [89] Muhammad Haris Zaffar, Shoab Ehsan, Michael Milford, and Klaus McDonald-Maier. 2021. VPR-Bench: An Open-Source Visual Place Recognition Evaluation Framework with Quantifiable Viewpoint and Appearance Change. *International Journal of Computer Vision* 129 (2021), 2136–2174. doi:10.1007/s11263-021-01469-5
- [90] Xiaohua Zhai, Basil Mustafa, Alexander Kolesnikov, and Lucas Beyer. 2023. Sigmoid loss for language image pre-training. In *Proceedings of the IEEE/CVF international conference on computer vision*. 11975–11986.
- [91] Gabriele Zhu, Carlone Luca, et al. 2021. Viewpoint invariant dense matching for visual geolocalization. In *IEEE/CVF International Conference on Computer Vision (ICCV)*. 12169–12179.
- [92] Sijie Zhu, Linjie Yang, Chen Chen, Mubarak Shah, Xiaohui Shen, and Heng Wang. 2023. R2Former: Unified Retrieval and Reranking Transformer for Place Recognition. In *Proceedings of the IEEE/CVF Conference on Computer Vision and Pattern Recognition (CVPR)*. 19370–19380.

## A Supplementary Materials for MMS-VPRLib

This section provides experimental details, model architectures, hyperparameter settings, and computational requirements for the MMS-VPRLib benchmark platform introduced in Section 4.

### A.1 Hyperparameter Configurations

As mentioned in Section 5, we use batch size 32 for most methods (except BLIP: 16, LR: 64). Table 5 details all model-specific hyperparameters (excluding common settings).

### A.2 Computational Resources

All experiments were conducted on a single personal laptop (no cloud or multi-node cluster).

#### A.2.1 Hardware Specifications.

- **Laptop model:** Lenovo Legion Y7000P IRX9
- **CPU:** Intel Core i7-14700HX (20 cores / 28 threads, base 2.1 GHz, L3 cache 33 MB)
- **GPU:** NVIDIA GeForce RTX 4060 Laptop GPU, 8 GB GDDR6
- **System memory:** 16 GB DDR5-5600 MT/s
- **Primary storage:** YMTC NVMe SSD, 1 TB
- **OS & drivers:** Windows 11 Pro 22H2 + WSL2 (Ubuntu 22.04), CUDA 12.5, cuDNN 9

**A.2.2 Runtime Analysis.** Table 6 reports training and testing time across all five datasets. Running any notebook on hardware comparable to an RTX 3060/4060 (8 GB) or higher is sufficient to reproduce the reported results.

### A.3 Code Repository

Complete implementation is available at <https://github.com/yiasun/MMS-VPRLib>. The repository includes:

- Jupyter notebooks for all 17 baseline models
- Conda environment files for reproducibility
- Complete training and evaluation scripts
- Data loading utilities for all supported datasets

Each notebook is self-contained and includes data loading, pre-processing, training, and evaluation steps. Exact commands and environment specifications are provided in the repository README.

## B Further Details of MMS-VPR Dataset

This section provides comprehensive supplementary materials for the MMS-VPR dataset, including related work, site details, collection protocols, data structure, statistical analysis, and usage instructions.

### B.1 Related Work in Visual Place Recognition

Visual Place Recognition (VPR) in urban street scenes has emerged as a critical task in autonomous navigation and geo-localisation. The quality, diversity, and realism of VPR models are fundamentally shaped by the datasets upon which they are trained and evaluated. This subsection reviews representative datasets in terms of their collection modalities, environmental scope, and sensor setups, as referenced in Section 1.

**Multisensor Robotic Platforms.** Datasets such as the University of Michigan North Campus dataset [15] exemplify multi-modal robotic mapping efforts. Leveraging a Segway-based platform, this

**Table 5: Hyperparameters for all 17 baselines.**

Model	Hyperparameter	Description	Value
ViT [29]	$d_{\text{embed}}$	Patch embedding dimensionality	64
	$L$	Number of Transformer layers	6
	$H$	Number of attention heads	8
	$d_{\text{mlp}}$	FFN hidden dimensionality	128
SVC [19]	$C$	Regularisation strength	1.0
RF [12]	$N_{\text{trees}}$	Number of trees	100
MLP [68]	$d_{\text{hidden}}$	Hidden layer sizes	(256, 128)
	$T_{\text{max}}$	Maximum iterations	300
LR [39]	$d_{\text{img}}$	Image branch hidden size	128
KNN [20]	$K$	Number of neighbours	5
GNB [52]	$\epsilon$	Variance smoothing	$1 \times 10^{-9}$
BoQ [3]	$l_{\text{pre}}$	Use pretrained backbone	True
SALAD [42]	$\lambda_{\text{distill}}$	Distillation loss weight	$5 \times 10^{-4}$
BLIP [47]	$p_{\text{crop}}$	RandomResizedCrop scale	(0.8, 1.0)
CLIP [66]	$L_{\text{unfreeze}}$	Unfrozen Transformer blocks	1
	$\phi$	Feature normalisation (L2)	True
EigenPlaces [10]	$p_{\text{GeM}}$	GeM pooling exponent	3.0
	$d_{\text{proj}}$	Projection dimension	256
	$\lambda_{\text{ortho}}$	Orthogonality regularisation	$1 \times 10^{-3}$
	$s$	CosFace scale factor	30.0
	$m$	CosFace margin	0.35
SFRS [27]	$r$	Channel reduction ratio	16
	$p_{\text{GeM}}$	GeM pooling exponent	3.0
R2Former [92]	$d_{\text{embed}}$	Token embedding dimension	256
	$L$	Transformer encoder layers	4
	$H$	Attention heads per layer	8
	$\rho$	MLP expansion ratio	4.0
	$\alpha_0$	Initial R2 fusion weight	0.5
PatchNetVLAD [32]	$d_{\text{proj}}$	Projection dimension	128
	$K$	NetVLAD clusters	16
	$\mathcal{G}$	Multi-scale grid sizes	[1, 2, 3]
	$R$	Total regions ( $\sum g^2$ )	14
MixVPR [2]	$d_{\text{proj}}$	Projection dimension	256
	$L_{\text{mix}}$	Number of Mix blocks	3
	$k_{\text{dw}}$	Depthwise conv kernel size	7
	$\rho$	Channel expansion ratio	2.0
	$p_{\text{GeM}}$	GeM pooling exponent	3.0
CosPlace [9]	$p_{\text{GeM}}$	GeM pooling exponent	3.0
	$d_{\text{feat}}$	Feature dimension	512
	$s$	CosFace scale factor	30.0
	$m$	CosFace margin	0.35

**Table 6: Training (Tr) and testing (Te) time across five datasets (minutes). Scaling: Tokyo  $\times 4$ , Pitt  $\times 10.26$ , New College  $\times 1$ , Nordland  $\times 4$ , Cambridge  $\times 1$ .**

Model	Tokyo		NewC		Pitt		Nord		Cambridge	
	Tr	Te	Tr	Te	Tr	Te	Tr	Te	Tr	Te
CLIP	45.9	8.1	2.1	0.4	252.8	44.6	146.2	25.8	7.7	1.3
BLIP	51.0	9.0	7.2	1.3	1002.5	176.9	571.2	100.8	12.8	2.2
BoQ	84.7	9.4	3.5	0.4	556.0	61.8	252.3	28.0	25.6	2.9
SALAD	81.8	9.1	3.5	0.4	876.0	97.3	425.8	47.3	16.3	1.8
ResNet	12.3	1.7	2.2	0.3	53.3	7.3	18.1	2.5	2.7	0.4
ViT	27.1	3.7	6.6	0.9	129.2	17.6	48.6	6.6	7.6	1.0
CosPlace	56.9	6.3	2.3	0.3	290.3	32.3	200.2	22.2	10.4	1.2
MixVPR	54.4	6.0	2.3	0.3	290.9	32.3	159.0	17.7	10.4	1.2
SFRS	55.8	6.2	2.4	0.3	295.8	32.9	165.6	18.4	10.6	1.2
EigenPlaces	54.8	6.1	2.3	0.3	288.3	32.0	159.8	17.8	10.1	1.1
PatchNetVLAD	54.6	6.1	5.0	0.6	291.7	32.4	160.1	17.8	10.4	1.1
R2Former	55.2	6.1	2.3	0.3	286.2	31.8	157.0	17.4	11.7	1.3

dataset integrates omnidirectional and planar LiDAR (Velodyne

HDL-32E, Hokuyo), IMU, fibre optic gyro, and RTK GPS, enabling robust support for long-term SLAM, obstacle detection, and appearance-based place recognition over 15 months of indoor and outdoor operations.

**Mobile Vehicle and Camera-Rig Systems.** For large-scale urban-scale datasets, vehicle-mounted camera rigs offer an efficient means of data acquisition. Chen et al. [18] constructed a 1.7M-perspective image dataset for landmark recognition by combining panoramic imagery and high-resolution cameras with GPS and inertial units. Similarly, NYU-VPR [72] employs smartphone cameras installed on fleet cars, capturing front and side views across day/night cycles to support privacy-preserving urban place recognition.

**Crowdsourced and Time-Machine Imagery.** The Mapillary datasets, both Mapillary Vistas [55] and Street-Level Sequences [83], utilise user-contributed imagery from smartphones, dashcams, and action cameras. These resources cover broad spatial and temporal variations, promoting semantic segmentation and lifelong recognition. GSV-Cities [1] collected from Google Street View Time Machine, offers 560K images with accurate GPS and bearing metadata spanning 14 years across 40 cities, making it particularly suitable for supervised VPR under appearance change and domain shift.

**Synthetic and Archival Imagery.** AmsterTime [87] integrates archival scans with modern street views through human-in-the-loop validation, enabling cross-domain VPR evaluation under extreme appearance shifts. HPointLoc [88] simulates indoor scenes via RGB-D rendering from Matterport3D, supporting indoor VPR and loop closure detection tasks without real-world image acquisition.

**Cross-View and Multi-Modal Datasets.** CV-Cities [41] and SpaGBOL [73] bridge ground-to-satellite geo-localisation by sampling panoramic street-view imagery alongside high-resolution aerial data. These datasets feature structured annotations of road-junction graphs, enabling spatial-graph-based orientation tasks and urban layout inference across cities and continents.

**Event-Based and Neuromorphic Imaging.** Recent advances in low-latency event sensors are reflected in the NYC-Event-VPR [59] dataset, which utilises a Prophesee HD event camera coupled with an RGB camera and GPS module mounted on vehicles. Covering over 260 km of New York City under diverse lighting and weather, this dataset supports exploration into neuromorphic vision systems for VPR.

**Indoor SLAM-Grade Benchmarks.** Indoor visual localisation datasets such as those by Lee et al. [46] use a sophisticated multi-sensor setup including Velodyne LiDARs, stereo cameras, IMUs, and wheel encoders to enable robust pose estimation and dense 3D reconstruction. These are particularly well-suited for robotics and AR-based visual relocalisation in cluttered environments.

**Urban Street Scene-Based VPR Methods.** MS-MixVPR [64] presents a multi-scale feature fusion architecture that combines ResNet50 with a FeatureReuse module to jointly encode local structures and global context, thereby enhancing robustness to typical urban variability such as seasonal changes and dynamic occlusions. MeshVPR [7] leverages synthetic city mesh reconstructions to train visual models using photo-realistic but cost-effective synthetic views. Hierarchical VPR [54] introduces semantic-guided attention using pretrained segmentation models (e.g., Mask2Former) to reweight image regions based on semantic salience. GICNet [84] further advances urban scene modelling through the Shuffle Channel

Attention module and the Global Information Aggregator, which extract globally consistent and context-aware features resilient to day-night and appearance variation.

## B.2 Site Selection and Characteristics

As introduced in Section 2.1, we selected Chengdu Taikoo Li for three key advantages: spatial openness, functional diversity, and urban integration. Here we provide additional details on site location and its advantages over indoor urban environments.

**B.2.1 Site Location and Spatial Layout.** Chengdu Taikoo Li is located in the CBD of Chengdu City, China. The development covers approximately 70,800 m<sup>2</sup>. As illustrated in Figure 7, the site comprises more than 40 two-to-three story individual buildings interconnected by a network of open-air pedestrian pathways that integrate seamlessly with surrounding urban streets.



**Figure 7: Boundary and spatial layout of the pedestrian streets within the site.**

**B.2.2 Advantages Over Indoor Mall Datasets.** Previous research on place recognition in urban commercial environments has primarily focused on interior spaces of conventional enclosed malls. For instance, Lee et al. [45] proposed a localization dataset of indoor shopping mall spaces in Seoul, South Korea. However, these datasets present several limitations:

- **Low visual diversity:** Interior mall spaces typically feature controlled, artificial lighting conditions with minimal temporal variation, limiting the model's ability to recognize identical places under different lighting environments.
- **Insufficient spatial uniqueness:** Interior commercial spaces, particularly brand stores (e.g., Louis Vuitton, Nike, Gucci), often employ standardized design languages across different locations worldwide. This lack of uniqueness impedes the development of place recognition algorithms with global applicability.
- **Limited environmental complexity:** Indoor environments lack natural variations in lighting, weather, and occlusion patterns that characterize real-world urban settings.
- **Restricted generalization:** Models trained on interior mall datasets may struggle to generalize to the diverse conditions found in outdoor urban environments.

**Table 7: Device specifications and raw data formats**

Device	Model	Output Image Format	Output Video Format
Smartphone	iPhone XS Max	4032×3024	1920×1080, 30 fps
Smartphone	iPhone 11 Pro Max	4032×3024	1920×1080, 30 fps

Our dataset addresses these limitations by focusing on outdoor pedestrian streets within an open-air commercial district. These spaces feature:

- **Environmental variability:** Comprehensive surrounding urban context features, skylines, natural lighting conditions, and varying pedestrian flows that ensure absolute and global uniqueness of place recognition results.
- **Semantic richness:** Varied functions including shopping, dining, leisure, art, and cultural spaces that provide diverse contextual cues for recognition.
- **Structural openness:** Long sightlines, rich occlusion patterns, and varied viewpoints that challenge and improve model generalization.
- **Temporal robustness:** Environmental variation across different times of day, weeks, months, seasons, and weather conditions, providing a more robust training foundation for place recognition algorithms.

The spatial configurations of these pedestrian pathways closely resemble urban public streets but with a more comprehensive layout of diverse commercial places for various daily activities. This makes it particularly suitable for examining the performance of place recognition algorithms in real-world urban scenarios with complex pedestrian dynamics.

### B.3 Data Collection Protocols

This subsection details the systematic data collection framework introduced in Section 2.3, providing implementation guidelines for reproducibility in other urban contexts.

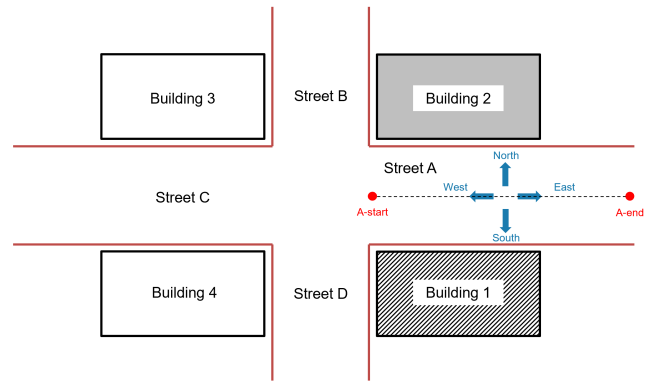
**B.3.1 Device Specifications.** To minimize equipment barriers and maximize reproducibility, we used only consumer smartphones for all data collection. Table 7 summarizes the device specifications and output formats.

In addition to smartphones, we utilized a simple handheld gimbal for video shooting, which helps stabilize the camera and provides smoother footage while reducing physical strain during extended recording sessions.

**B.3.2 Four-Direction Coverage Implementation.** As introduced in Section 2.3, we capture from four cardinal directions (N, S, E, W) for each street location. Figure 8 illustrates the framework for collecting visual features from different directions.

Taking street A as an example, the collection procedure is:

- (1) With camera facing East, walk from "A-start" to "A-end," recording videos to capture spatial features visible when walking eastward.
- (2) With camera facing North (toward Building 2), walk from "A-start" to "A-end," recording videos to capture the facades of buildings on the north side of street A.

**Figure 8: Guidelines for collecting visual features from four directions on a street.****Table 8: Field of view comparison between smartphone cameras (iPhone 11 Pro Max) and human eyes.**

Apparatus	Mode	Lens	Horizontal FOV	Vertical FOV
Smartphone	0.5×	Ultra-wide lens	~120°	~90°
	1×	Wide lens	~65°	~46°
Human eyes	N/A	N/A	~120°	~60°

- (3) With camera facing West, walk from "A-end" to "A-start," recording videos to capture spatial features visible when walking westward.
- (4) With camera facing South, walk from "A-end" to "A-start," recording videos to capture the facades of buildings on the south side of street A.

**B.3.3 Dual-Perspective Capture Implementation.** As described in Section 2.3, we employ two shooting angles to simulate human viewing behaviors in high-rise urban settings:

- **0° horizontal angle:** Representing the standard forward-looking perspective when walking, capturing typical eye-level architectural features.
- **45° upward angle:** Simulating the natural head tilt when observing tall buildings, capturing upper-level urban context and building skylines.

Table 8 compares the field of view between smartphone cameras and human eyes.

**B.3.4 Temporal Coverage Strategy.** As introduced in Section 2.3, we enforce balanced temporal coverage during daytime (7AM–5PM) and nighttime (6PM–10PM) periods. We also identify three fine-grained daytime intervals—early morning, noon, and twilight—each offering unique visual features (Figure 9):

- **Early Morning (7–9 AM):** Most stores remain closed, and pedestrian traffic is minimal. This results in low occlusion of architectural elements, making this period ideal for capturing unobstructed urban features.
- **Noon (12–2 PM):** Pedestrian volume peaks as office workers take lunch breaks. Crowded conditions cause significant



Figure 9: Street scenes during three daytime periods: early morning, noon, and twilight.

Table 9: Characteristics of pedestrian street visual features at different times

Period	Sub-period	Time frame	Pedestrian occlusion	Lighting
Daytime	Early morning	07:00–09:00	Minimal	Daylight
	Noon	12:00–14:00	Moderate to maximal	Daylight
	Twilight	17:00–19:00	Moderate to maximal	Daylight + artificial
Nighttime	N/A	19:00–22:00	Moderate to maximal	Artificial

occlusion of architectural scenes, providing valuable data for training place recognition under partially obstructed views.

- **Twilight (5–7 PM):** This is a transitional phase where daylight gradually diminishes and artificial lights are activated. The coexistence of ambient skylight and artificial illumination offers a mixed-light environment.

Table 9 summarizes the characteristics of visual features across different time periods.

### B.4 Dataset Structure and Encoding

As described in Section 3, our dataset organizes 208 locations using a graph-based spatial encoding system. Here we provide detailed encoding methodology and spatial organization.

**B.4.1 Spatial Encoding Methodology.** Each location receives a unique identifier preserving geographic coordinates and spatial relationships. Figure 10 illustrates examples of how each place type is encoded on the map.

The encoding follows these systematic principles:

- **Horizontal Streets (Edges):** Encoded as "Eh-*i*-*j*" where *i* indicates row number (top to bottom) and *j* indicates column number (left to right) within that row.
- **Vertical Streets (Edges):** Encoded as "Ev-*n*-*m*" where *n* indicates column number (left to right) and *m* indicates row number (top to bottom) within that column.
- **Intersections (Nodes):** Encoded as "N-*i*-*j*" where *i* indicates row number and *j* indicates column number.
- **Squares (Open Areas):** Encoded as "S-*r*" where *r* indicates the rank by area (1 for largest).

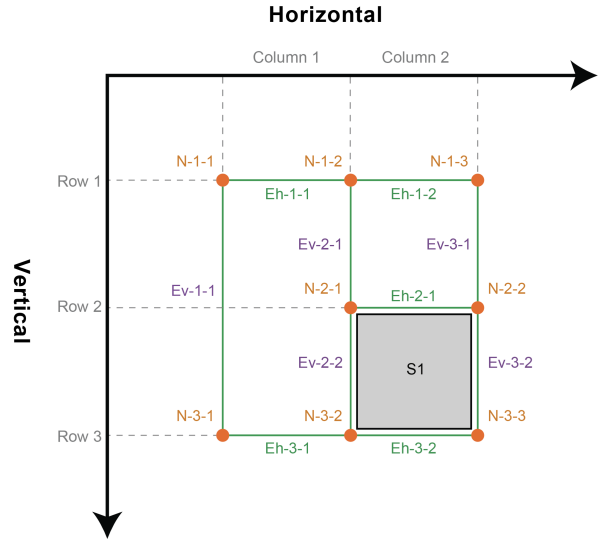


Figure 10: Encoding examples of different place types.

This hierarchical encoding preserves both geometric position and topological relationships, enabling construction of adjacency matrices and distance metrics for graph-based learning algorithms.

**B.4.2 Geographic Distribution.** Figure 11 visualizes the geographic distribution of all 208 locations in the dataset, illustrating the spatial relationships between different place types and their coverage across the precinct mall.

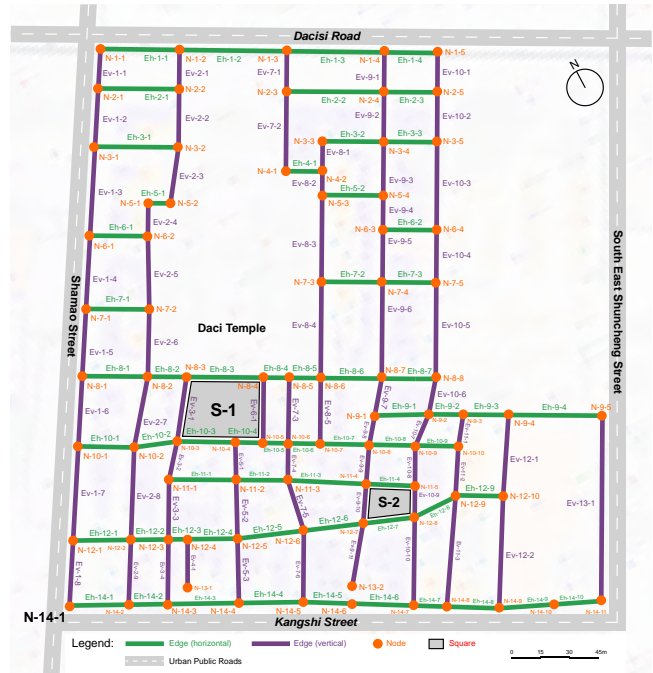


Figure 11: Geographic distribution of all 208 places in the dataset.

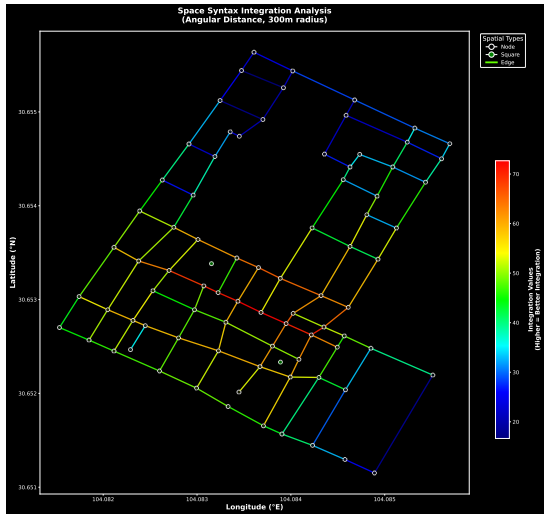


Figure 12: Integration metric visualized on the MMS-VPR pedestrian network. Warmer colors = higher accessibility.

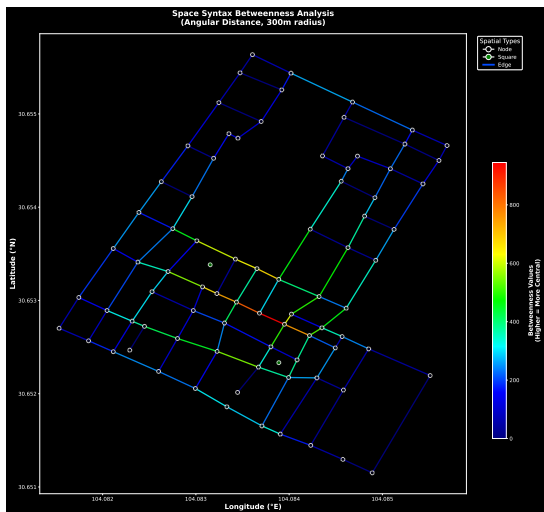


Figure 13: Betweenness metric visualized on the MMS-VPR pedestrian network. Warmer colors = larger pedestrian flows.

## B.5 Space Syntax Metric Visualizations

As introduced in Section 3.3, we compute space syntax metrics to quantify spatial accessibility and movement potential for each location. Figures 12 and 13 visualize these metrics across the MMS-VPR pedestrian network. They reveal clear hierarchical spatial structure: central corridors (red/orange, high values) attract pedestrian movement and serve as primary navigation routes, while peripheral alleys (blue, low values) provide localized access. This spatial hierarchy aligns with observed pedestrian flow patterns in the study site, validating the utility of space syntax metrics for predicting movement potential and supporting future research on flow-aware VPR and hierarchical place retrieval.

## B.6 Dataset Access and Usage

The complete MMS-VPR dataset is publicly available at <https://huggingface.co/datasets/Yiwei-Ou/MMS-VPR>. The dataset is provided in a preprocessed version with standardized resolution (images: 256×192; videos: 256×144 at 30fps), totaling approximately 11 GB distributed across four modality-specific archives. Detailed documentation on data organization, file structure, annotation schemas, and graph topology can be found in the repository.

**B.6.1 Download Instructions.** The dataset is split into four components to support flexible, bandwidth-efficient access:

```
# Download all components (~11 GB total)
wget https://huggingface.co/datasets/Yiwei-Ou/\
MMS-VPR/resolve/main/Images.tar.gz
wget https://huggingface.co/datasets/Yiwei-Ou/\
MMS-VPR/resolve/main/Videos.tar.gz
wget https://huggingface.co/datasets/Yiwei-Ou/\
MMS-VPR/resolve/main/Texts.tar.gz
wget https://huggingface.co/datasets/Yiwei-Ou/\
MMS-VPR/resolve/main/Graph_Structure.tar.gz
```

```
# Extract all archives
tar -xzf Images.tar.gz
tar -xzf Videos.tar.gz
tar -xzf Texts.tar.gz
tar -xzf Graph_Structure.tar.gz
```

Researchers requiring only a subset of modalities may download components selectively: `Images.tar.gz` (~2.25 GB), `Videos.tar.gz` (~8.78 GB), `Texts.tar.gz` (~417 KB), and `Graph_Structure.tar.gz` (~112 KB). Original high-resolution data (images: 4032×3024; videos: 1920×1080) are available upon reasonable request for specialized applications.

## B.7 Licensing and Ethics

**B.7.1 License.** The dataset is released under the Creative Commons Attribution 4.0 International (CC BY 4.0) license, permitting use, sharing, and adaptation for any purpose, including commercial applications, with appropriate attribution. All data were collected and curated by the authors without using third-party copyrighted material.

**B.7.2 Ethics Statement.** Our research adheres to ACM and KDD ethical guidelines. All data were collected in publicly accessible outdoor commercial spaces (pedestrian streets and open-air shopping plazas) during daytime and evening hours. Data acquisition followed strict ethical principles:

- **Privacy Protection:** All identifiable information including faces and license plates were automatically detected and anonymized through pixelation. No private interior spaces or restricted areas were captured. All media underwent manual review to verify complete removal of personally identifiable information (PII).
- **Public Space Only:** Collection was strictly limited to publicly accessible outdoor areas where pedestrians naturally expect to be observable, avoiding any surveillance of private or semi-private spaces.

- **Pedestrian-Level Viewpoints:** Data were captured using handheld consumer devices at natural eye level (horizontal and upward perspectives), avoiding invasive elevated or surveillance-style viewpoints that could compromise privacy expectations.

- **Spatial and Temporal Coverage:** To ensure unbiased and representative data, collection was conducted from four cardinal directions at each location across varied lighting conditions (daytime and nighttime), while avoiding intrusion during late-night hours.

The dataset is designed to support research in multimodal place recognition, urban analytics, and navigation systems while fully respecting privacy rights and public ethics standards.